Sampling depth in conversion-electron detection used for x-ray absorption

T. Girardeau, J. Mimault, M. Jaouen, and P. Chartier
Laboratoire de Métallurgie Physique, URA 131 CNRS, 40 Avenue du Recteur Pineau, 86022 Poitiers, France

G. Tourillon
Laboratoire d'Utilisation du Rayonnement Electromagnétique, Bâtiment 209D, 91405 Orsay CEDEX, France
(Received 29 October 1991)

Several x-ray-absorption K thresholds have been measured for thin-film specimens in helium gas. The data are analyzed in terms of the different types of electrons that are ejected out of atomic cores in x-ray-absorption events and their relative contribution to the output signal. Theoretical expressions are derived that predict the K-edge yield as a function of the thickness, density, and atomic concentration of the specimen and as a function of the K-edge nature. Fits yield values of the coefficients in these expressions for samples irradiated with x rays with energy in the 5–10-keV range.

I. INTRODUCTION

Protective coatings are generally used to improve the tribological performance of mechanical components. They resist chemical corrosion or delay degradation induced by friction. They are often used to improve the lifetime of substrates while contributing to mechanical properties of the assembly. Applications of coatings to metallurgical tools usually involves very thin deposited films; ion implantation can also play a useful role in their mechanical protection. Therefore, the microscopic structure of such coatings must be well characterized in order to determine the criteria for an optimized protective layer. So, typical surface experiments are required in the investigation of coating intrinsic properties.

Extended x-ray-absorption fine structure (EXAFS) measurements are nondestructive and yield information about local atomic structure. Surface EXAFS apparatus operates without direct contact with the specimen in order to avoid modification of the film-substrate region. The sampling depth must be in agreement with the coating thickness, and we have to perform the measurements with an appropriate experimental method. Metallurgists are generally concerned with effective coating depths, which typically vary between several nanometers and one hundred nanometers. The conversion electron device can be considered as a suitable EXAFS detector in order to probe such a specific depth field, but the sampling depth varies with the nature of excited atoms and with the overlayer structure. In order to clarify this point, the present paper focuses on the results provided by the total-electron-yield technique previously described by Kordesh and Hoffman.[1] In particular, the behavior of the probed depth was carefully analyzed for different K edge atomic thresholds by examining signal magnitude (pre-edge and edge data) versus film thicknesses. Several sets of samples were studied and then their experimental behaviors were correlated with the kinetic energy of the "primary electrons." As primary electrons, we design either photoelectrons or Auger electrons extracted from the atomic potential during photoabsorption or nonradiative deexcitation events. The investigation has been limited to the x-ray K absorption by elements belonging to the first transition row of the Periodic Table for which a majority nonradiative deexcitation process occurs.

The goals of the present paper are twofold. First, we wish to discuss the accuracy of the empirical relation generally used to determine the "escaping depth," i.e., the effective depth representative of the signal measured in conversion-electron yield experiments. To do this, we propose an analytical relation in order to describe the conversion-electron signal magnitude. Second, we give the numerical values of the coefficients involved in this formulation, which fit the experimental results obtained in the 5–10-keV energy range investigated in this work.

The data presented here have been obtained at the Laboratoire pour l'Utilisation du Rayonnement Electromagnetique (LURE) at Orsay on the DCI storage ring using the conversion-electron detector developed by Tourillon *et al.*[2] The experimental setup uses a monochromator (channel-cut on beamline EXAFS1, double crystals on beamlines EXAFS3 and EXAFS4), an ionization chamber filled with a He-Ne gas mixture in order to measure the incident photon intensity I_0, and the conversion-electron detector itself. This last device essentially consists of a chamber filled with He gas and by an electrode positively biased with respect to the sample put at the electrical ground. The detector current is sent to a Keithley picoamperemeter. Under x-ray irradiation, the sample surface emits a bunch of electrons which are distributed over a rather broad kinetic-energy range with an upper limit defined by the primary electron energy E_p. The energy-distribution function occurs because of inelastic and elastic scatterings that affect the electron migration towards the free sample surface. This phenomenon depends on the atomic structure and its magnitude is generally expressed through the specific density τ of the scattering medium. The He gas filling the detector enhances the signal-to-noise ratio; in fact, an electron escaping from surface creates a sequence of He^+ ion–electron pairs until its kinetic-energy loss and, therefore, its contribution to the collected signal is assumed to

be proportional to its initial energy. Hence, among escaping electrons, the most energetic contribute most to the signal, and one may assume that the sampling depth is primarily sensitive to the high-energy part of the escaping electron energy spectrum. Several experimental works[3-7] have attempted to get information about the sampling depth, in particular its behavior against the material density and the K-edge nature. They tried to derive a practical expression which correctly describes the emission depth profile. From these studies, it seems that the electronic signal decreases exponentially as the primary photoabsorption event occurs far away from the free surface. Such behavior has been stated for particular experiments where an initial electronic current I_i, provided by a layer of x-ray-absorbing atoms, is then scattered by an additional overlayer material.[4] The measured current is then fitted by the expression $[I(z)=I_i\exp(-z/D)]$, z being the overlayer depth and D an effective escaping depth. This last parameter is at once a function of I_i, or more directly of the escaping electron energetic distribution, as well as the overlayer scattering power efficiency.

The experiments we perform are somewhat different because both x-ray absorption and electron-scattering phenomena occur inside the coating itself, which is depth limited. Then, the parameter D is only specific to the measured film; but one may have to account for a bulk contribution when both coating and substrate contain the same excited atomic species.

II. CONVERSION ELECTRON YIELD EXPRESSION

If we consider a slice of infinitesimal thickness dz lying at the free surface of the x-ray-irradiated sample, we can reasonably assume that primary photoelectrons and Auger electrons, created inside that slice, have the maximum probability to escape directly in the He gas filling the detector chamber, without energy loss. Nevertheless, we must also take into account that primary electrons which initially travel towards the opposite direction (i.e., distributed over 2π sr) may be backscattered by atoms lying much deeper inside the film. Such electrons have a significant probability to exit in the He gas, or to produce secondary electrons, after they have undergone inelastic collisions induced by underground atoms. Therefore, due to these additional phenomena, the exit-electron energy spectrum is extended over a rather broad energy range lying below the value E_p previously defined. However, one can expect that the integrated energy issued from this slice surface reaches the maximum value when compared to those related to deeper slices defined with the same thickness. The electronic current born of primary electrons created inside the slice surface must be correlated to E_p and to the sample topology. In order to write a simplified relationship, we assume the current to be proportional to E_p, the proportionality factor being dependent on the probed sample density. Further experimental analysis will show the validity of such a proportionality assumption; it also depends on the irradiated surface of the specimen.

The conversion-electron EXAFS detector works at high enough voltage (60 V) to keep out atomic recombination during charge transfer to electrodes. Its efficiency behavior is expected to be like that of the incident x-ray beam ionization chamber. In the unsaturated regime, it is well known that efficiency remains proportional to the energy of the incoming particle, since ion-electron pairs are produced until they come to rest in the gas filling the chamber. Nevertheless, primary electrons are created inside the sample and suffer electrostatic interactions before they escape in the He gas filling the detector, while in the ionization chamber, electrons are directly ejected in the He-Ne gas by photoionization of Ne atoms. Then, for this last device, one may assume that K photoelectrons and subsequent Auger electrons together yield a total kinetic energy which approaches E_i, the incident x-ray-beam photon energy.

With these assumptions the signal from the front surface slice of infinitesimal thickness dz, characteristic of the primary electron energy E_p, can be expressed in the following way:

$$dS(E_i,E_p,\tau,z=0)=\frac{dI(E_p,E_i,\tau)}{I_0(E_i)}=k\frac{E_p}{E_i}\frac{\mu_s(E_i)}{\mu_{\mathrm{Ne}}(E_i)}\frac{dz}{h_0}\ , \tag{1}$$

where $\mu_s(E_i)$ denotes the sample absorption cross section which is responsible for the primary electron (energy E_p) creation, whereas $\mu_{\mathrm{Ne}}(E_i)$ is the absorption cross section of Ne atoms filling the I_0 detection chamber which active length is h_0.

When the infinitesimal slice is taken deeper, electrons undergo amplified scattering effects when traveling through the material before reaching the free surface. Compared with the previous elementary signal (1), the contribution of such a slice is weaker, and when the resulting energy loss is approximated by an exponential decay law, it gives rise to an escaping depth D. In order to clarify the meaning of D and to predict its behavior versus x-ray energy and sample structure, we have performed various experiments by multiplying x-ray absorbing elements and solid structure types.

Our results and discussion about them are based on four sets of metallic specimens; their characteristics are summarized in Table I. They essentially consist of the following.

Different WO_3 overlayer thicknesses deposited by ion sputtering[8] on Cu foils of uniform thickness.

Different thicknesses of copper evaporated on quartz substrates by the same technique that were covered by a very thin WO_3 overlayer to prevent Cu oxidation.

Crystalline Fe-Co alloys which were obtained by using a dual-electron-beam system.[9]

Amorphous Ni-Ti alloys deposited on quartz substrates by a sputtering technique.

Deposited thicknesses were determined by a quartz crystal microbalance. Additional measurements performed with an x-ray reflectivity apparatus[10] on some samples we

TABLE I. Summary of the different samples evaporated on quartz substrates and experimented upon in the electron-conversion device.

Sample	Layer thickness (nm) 2.5	5	10	20	40	80	125	160	K edge
W/Cu(10 nm)	×		×	×	×	×			Cu
W(2.5 nm)/Cu		×	×	×	×	×		×	Cu
(Fe-Co)		×	×	×	×	×	×		Fe and Co
(Ni-Ti)		×	×	×	×		×		Ni and Ti

used enable us to obtain a percentage error on the thickness of about 5%, a value which is overestimated.

X-ray absorption spectra were recorded at LURE on the DCI storage ring operating at 1.96 GeV with a current of 300 mA. All samples were probed under identical conditions; substrate format, position, and orientation with respect to the x-ray beam; spectroscopic rate and picometer sensitivity are kept constant, at least for samples belonging to the same family. Errors occurring in the determination of the signal heights are generated by some possible change of the experimental conditions, the sample orientation being the main one. Error bars played on Figs. 2–4 have been estimated from a possible disorientation of 0.5° of the surface sample with respect to photon-beam direction. The results have been slightly emphasized in order to take into account any variation of the gas pressure in the detection device.

III. K-EDGE JUMP BEHAVIOR

A. Cu-based materials

We have begun our investigations by systematic measurements performed in order to determine the actual decay law caused by additional scattering layers. The underlayer active material is a Cu film, the thickness of which is kept constant for all sample classes, recovered by evaporated W-based material. These two elements were chosen because of their well-known immiscibility properties. X-ray reflectometry[10] and glancing-angle scattering experiments[11] reveal that the overlayer is essentially made up of WO_3 crystallites. Its density was experimentally estimated to be 13.75 g/cm^3.

The signal behavior was exclusively studied on Cu K-edge jump data because the current is mainly due to the energetic KLL Auger electrons (7 keV). Pre-edge amplitudes result from several contributions, essentially the Cu L and W M primary photoelectrons, whose contributions evolve in the opposite way when the WO_3 thickness increases. The I_0 damping provided by photoabsorption inside the WO_3 layer never goes beyond 1.5% and is easily amended. On Fig. 1 are plotted the $\ln[S_K(z)]$ data, the parameter z labeling the WO_3 overlayer thickness. These results confirm that the detection mechanism involved in the detector used here approximately acts in the expected way: one can consider that a decreasing exponential law correctly matches the behavior of the Cu K-edge jump when an increasing overlayer thickness (here WO_3 constituted) is recovering the x-ray active film (here Cu constituted). The best fits with the exponential form $S_K(z)=S_K(0)\exp(-z/D)$ are achieved with $D_{WO_3}=44$ nm. This value is, at once, significant of the energy E_p, the finite Cu-layer thickness, and the W-based material topology. So, from this kind of experiment it is rather complicated to extract any precise conclusion about the relationship linking D and physical parameters.

Therefore, we turn to a more simplified problem by considering a finite thickness of absorbing material as being a stacking of successive infinitesimal slices. Each of them yields a deceasing contribution to the total signal, the further away from the surface they lie. To test this scheme, the elementary observation consists in measuring the signal behavior versus the sample thickness. Such an experimental setup allows us to assess the contribution of slices lying deeper and deeper with respect to the one located at the free surface.

Owing to the exponential decay law quoted above, an infinitesimal slice located at depth z supplies an elementary signal defined by

$$dS(z)=dS(0)\exp(-z/D) .$$

Then, for a depth-limited film, one can derive the following expression:

$$S(E_i,E_p,\tau,z_0)=S(E_i,E_p,\tau)[1-\exp(-z_0/D)] , \quad (2)$$

where z_0 is the probed film thickness, while $S(E_i,E_p,\tau)$ denotes the signal related to large thicknesses ($z_0 \gg D$),

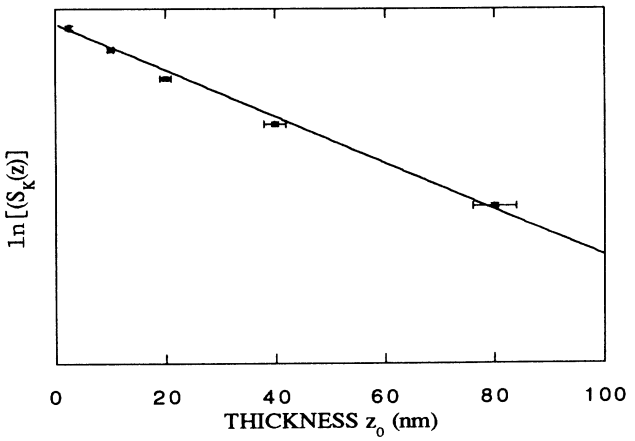

FIG. 1. Square: experimental log of Cu K-edge electron yield plotted vs WO_3 overlayer thickness (for constant Cu-layer thickness). The full line slope is 1 over 44 nm.

$$S(E_i,E_p,\tau)=\frac{I(E_p,E_i,\tau)}{I_0(E_i)}=k\frac{E_p}{E_i}\frac{\mu_s(E_i)}{\mu_{\mathrm{Ne}}(E_i)}\frac{D}{h_0}\ . \quad (3)$$

In this last expression, D can be viewed as a fictional thickness for which each of its x-ray-absorbing centers yields the escaping-electron spectrum characteristic of the free surface infinitesimal slice. Figures 2(a) and 2(b) show the experimental Cu K-edge jump behavior versus the evaporated Cu film thickness. Using Eq. (2), a least-square-root method leads to the best fit with the data for $D_{\mathrm{Cu}}=59$ nm.

For both previous experiments, primary Auger electrons have the same energy (7 keV), and the ratio $D_{\mathrm{Cu}}/D_{\mathrm{WO_3}}$ must be essentially dependent on density and lattice structure differences occurring between Cu and WO_3 material. In the literature,[3,5] the electron escaping depth was always assumed inversely proportional to the specimen density τ. Direct application of such an assumption provides a misfit percentage of about 15% in the present case. This miscorrelation, which shows the crudeness of the model, may be due to the dissimilarities between the two experimental setups. In particular, we must remember that the copper film is depth limited in the first experiment described above, so that it results in a specific outgoing electron energy spectrum, these electrons being thereafter scattered by the WO_3 overlayer. This energy distribution is undoubtedly different from that given by an infinitesimal free surface slice that constitutes the reference for the current decay observed for deeper slices in the second experiment set.

B. Alloys

Uniform alloys provide access to several k edges, and therefore to different Auger electron energies, for the same structural topology. So, one can deduce directly unambiguous information about the relationship that exists between the escaping depth D and the primary energy E_p. In particular, the semiempirical law $D=K_0E_p^{\alpha}/\tau$ generally quoted in the literature[3-5] (where K_0 is a constant) can be tested confidently when one performs experiments on several alloys, each of them providing a value

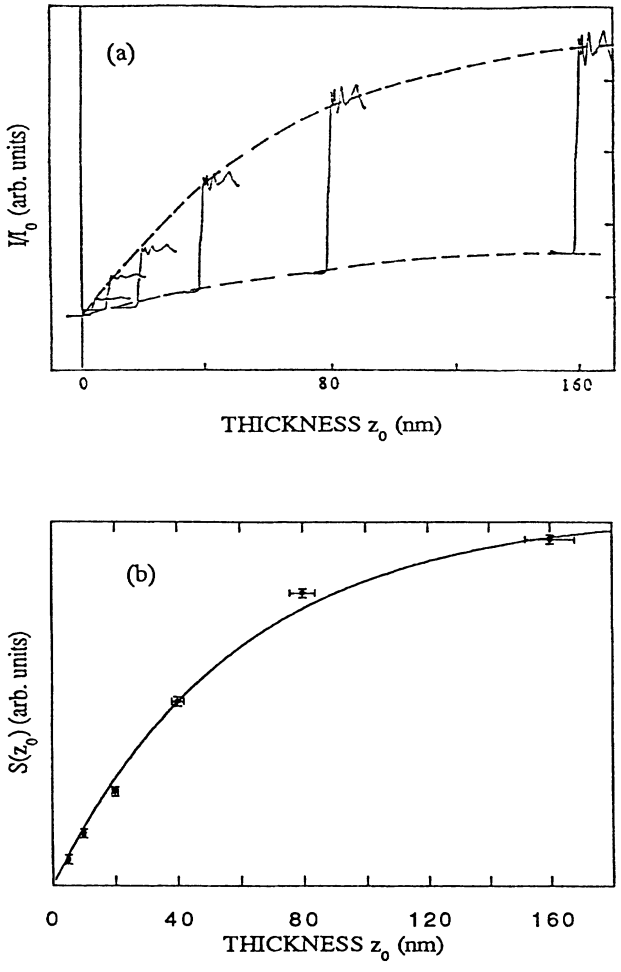

FIG. 2. (a) Cu K-edge absorption signal vs the thickness of Cu-deposited layer on quartz substrate. (b) Cu K-edge step height vs the Cu deposited layer thickness. Fit corresponds to $D=59$ nm.

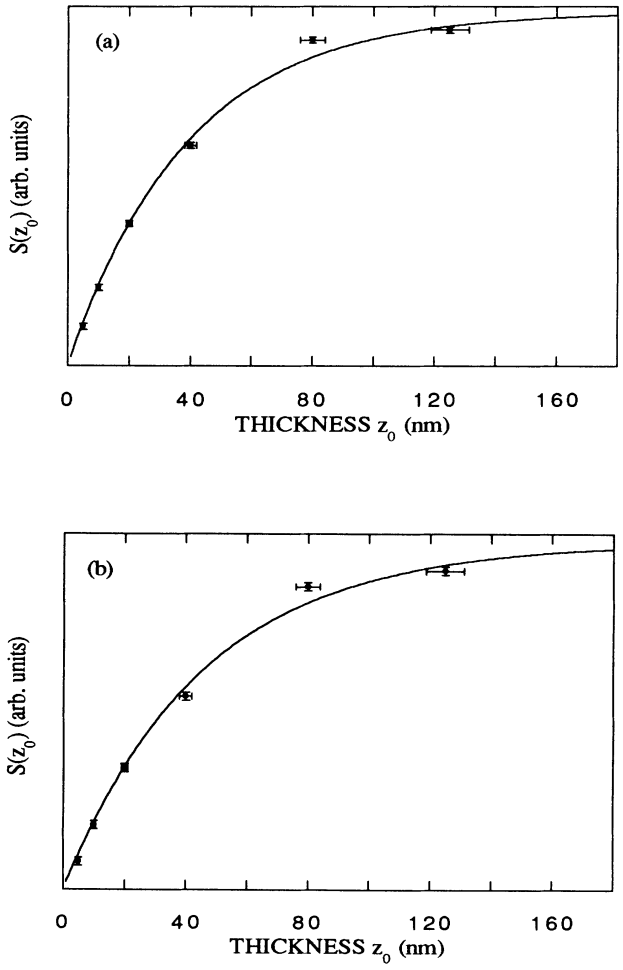

FIG. 3. K-edge step height vs Fe-Co alloy-deposited layer thickness. (a) Fe K edge fit corresponds to $D=39$ nm. (b) Co K edge fit corresponds to $D=46$ nm.

of coefficient α extracted from data. With this aim in mind, films of Ni-Ti and Fe-Co were deposited on quartz substrates and acted on conversion-electron by the EXAFS device. Although the evaporated compositions differ slightly from those originally programmed, all layers (Ni-Ti or Fe-Co) were elaborated under the same technical conditions and are expected to have, whatever the thickness is, identical composition and microstructural topology. Fe-Co alloys are cubic centered and chemically ordered, while Ni-Ti samples are amorphous. Experimental ratios $D_{\mathrm{Fe}}/D_{\mathrm{Co}}$ and $D_{\mathrm{Ni}}/D_{\mathrm{Ti}}$ were extracted from the data following two distinct ways.

(i) Each K-edge jump curve was fitted by the exponential law (2) previously mentioned, resulting in an absolute escaping depth for each K edge. Fits are plotted on Figs. 3(a) and 3(b) for Fe and Co K edges and Figs. 4(a) and 4(b) for Ni and Ti ones. Here one can notice again adequacy of the relation (2).

(ii) Experimental ratio curves $[S_A(z)/S_B(z)]$ were plotted on Figs. 5(a) and 5(b) (A and B stand for A-B alloy). Combining Eqs. (1) and (3), one can derive the following relation in a straightforward way:

$$\frac{D_A}{D_B}=\frac{(S_A/S_B)_{z\to\infty}}{(S_A/S_B)_{z\to 0}} . \tag{4}$$

The determination of such a quantity is easily allowed by the extrapolation of the experimental curves. Both methods yield practically identical ratios D_A/D_B. Results are gathered in Table II; those related to the Cu K edge and quoted above are also reported as well as the different primary electron energies E_p involved in x-ray atomic absorption events, electrons which are specific to each sample class. As discussed before, several Auger electrons emitted in cascade connection are needed to achieve atomic nonradiative deexcitations. In the energy range explored here, only *KLL* and *LMM* Auger electrons may have a significant weight. Their energy values have been approximated in the following way. *KLL* Auger electrons are peaked around a mean characteristic energy $E_p=(E_K-2E_L)$ with $E_L=(E_{L1}+E_{L2}+E_{L3})/3$. The energy of the subsequently emitted *LMM* Auger electron is very close to E_L.

However, one can ask a question about the energy value which must be involved in the relationship $D=K_0E_p^{\alpha}/\tau$. Is the experimental escaping depth only significant of the most energetic primary electrons or of the overall energy $E_T=\sum_n E_{pn}$ exchanged during nonradiative atomic deexcitation? Fortunately, as shown by

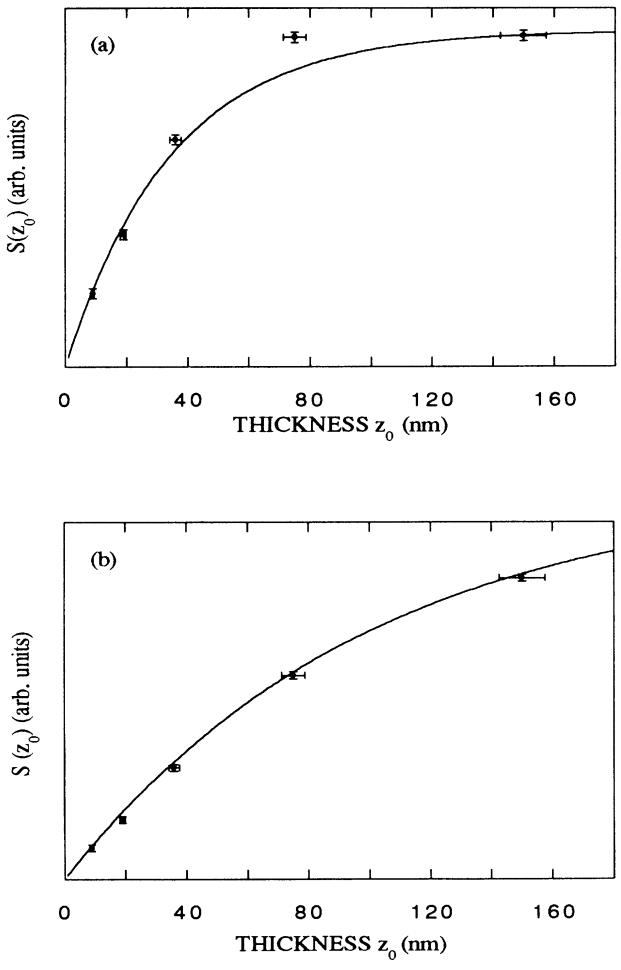

FIG. 4. K-edge step height vs Ni-Ti alloy-deposited layer thickness. (a) Ni K-edge fit corresponds to $D=100$ nm. (b) Ti K-edge fit corresponds to $D=35$ nm.

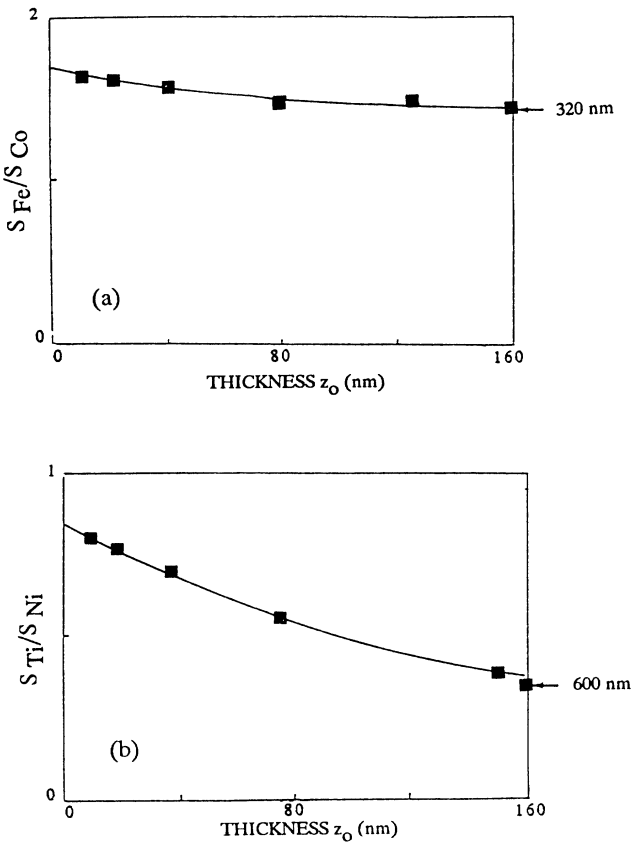

FIG. 5. K-edge ratio behavior vs the film deposited thickness. (a): S(Fe K edge)/S(Co K edge). (b): S(Ti K edge/S(Ni K edge).

TABLE II. Parameters included in the semiempirical relation $D=K_0E_p^{\alpha}/\tau$ and calculated by fitting experimentally K-edge height behavior vs deposited sample thickness. D_A/D_B is extracted from the data by (i) fit of the K-edge jump curve by the exponential law $S(z_0)=S_{\infty}[1-\exp(z_0/D)]$ and (ii) extrapolation of the $S_A(z)/S_B(z)$ curve.

Sample	Edge	E_p (keV)	$\sum_n E_{pn}$ (keV)	D (nm)	(D_A/D_B) (i)	(D_A/D_B) (ii)	α	τ (g/cm^3)	K_0
Cu	Cu	7	8	59				8.96	73
Fe-Co	Fe	5.6	6.35	39	0.84	0.82	2.18	8.3	73
	Co	6.04	6.85	46					
Ti-Ni	Ti	4	4.5	35	0.35	0.34	2.23	5.1	84
	Ni	6.4	7.3	100					

numerical values quoted in Table II, the ratio E_p/E_T remains approximately constant whatever the excited element was, owing to the similar energy behavior of K and L core levels for transition elements of the Periodic Table; so, the α value that results is not appreciably changed.

In spite of their rather different ratio E_A/E_B and microstructural topology, Ni-Ti and Fe-Co materials predict very close values for the exponent α. So, we can conclude from the analysis that the empirical rule $D=K_0E_p^{\alpha}/\tau$ may be used for $\alpha=22$, in the 5–10-keV energy range studied here.

To allow us to observe, at least qualitatively, the reliability of the predicted $(1/\tau)$ behavior of the escaping depth D, a last column has been added in Table II. The density of Fe-Co samples was calculated by starting from the concentration measured by electron microscopy microanalysis. It is more difficult to estimate the density of Ni-Ti films in the same way, owing to their amorphous character, so we used the x-ray reflectometry apparatus in order to obtain a more reliable value. Calculations on different crystalline materials yield the same coefficient, but an obvious misfit is observed for the amorphous state: if one tries to reach the specific crystalline value, the corresponding density of the amorphous Ni-Ti material must be lowered to a physically nonsensical value unless partial oxidation of the surface exists. However, this possibility must be disregarded owing to the threshold and low-energy EXAFS signal forms. Therefore, the experimental data obtained here suggest that the escaping depth increases when the mater condenses in its amorphous phase. A possible explanation of such a particular behavior might be that the scattering process becomes more efficient in amorphous materials, so that they give rise to an enhanced statistical weight of lower-energetic secondary electrons for which, as is well-known, the mean free path is greater. To confirm this assumption it would be necessary to perform additional experiments on various amorphous materials.

IV. SIGNAL INTENSITY BEHAVIOR

Expressions (1) and (3) have been derived in order to predict the material depth analyzed by the conversion-electron EXAFS apparatus. Absolute values have been extracted from experimental K-edge amplitude behaviors that have been plotted independently for each class of materials. Moreover, a more precise analysis can be also developed in order to link escaping depth and energies of the different primary electrons simultaneously involved in the x-ray-absorption process. This can be achieved by comparing electronic intensities yielded by different materials; such computations will also allow us to discuss the validity of the assumptions involved when writing down Eq. (1). First, attention will be paid to absolute electronic current values issued from a sample or substrate for the same x-ray beam energy E_i, so that the comparison remains independent of the I_0 measure. Second, we shall focus on the E_i variation effect on the signal intensity by performing a careful comparison between theoretically computed and experimental pre-edge slopes.

A. Electronic current intensities

Calculations are restricted to data collected just before Ti, Fe, and Cu K edges. For these precise materials, electron yields result from L photoelectrons and LMM Auger electrons, while for SiO_2 substrates, K photoelectrons, KLL and LMM Auger electrons are involved in an x-ray absorption event. Ni K (and Co K) pre-edge implies a rather more complicated electron set because, in the present alloys, additional K photoelectrons and KLL Auger electrons come from Ti (or Fe) excited atoms.

Hence, we are interested in the thin-film to substrate current ratios. They were experimentally carried out by plotting the pre-edge data, collected at about 50 eV before the edge jump, versus the deposited thickness. The results are shown on Fig. 6 for Fe and Ti L absorption; one can also look at Fig. 2(a) for the Cu K edge pre-edge behavior. An extrapolation of these curves allows us to obtain the substrate and bulk sample results for $z\rightarrow\infty$ and $z\rightarrow 0$ signals. The extrapolation method reduces the error risks on the extreme values needed to calculate the ratio, relative to that provided by only two distinct experiments; moreover we avoid the difficulty which may occur owing to the insulating character of SiO_2 substrate; indeed, a measurement performed on SiO_2 alone makes the result questionable, because positive charges can accumulate quickly on insulating materials.

Using Eq. (3), which is well adapted to large thicknesses, one can perform straightforward computa-

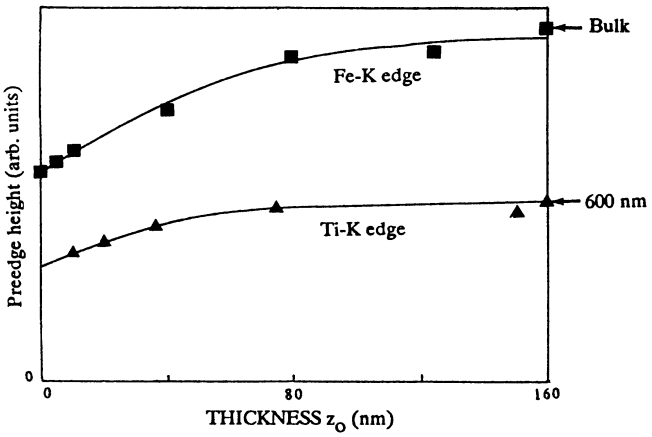

FIG. 6. Ti and Fe K pre-edge absorption height vs the deposited alloy thickness.

tions by starting from different possible conceptions of the escaping depth D derived from experiments; two ways were investigated.

(i) We assume that D must be expressed in terms of the total energy E exchanged by outgoing electrons during excitation and deexcitation steps. Consequently, for L photoabsorption (Ti, Ni, Fe, Co, and Cu atoms), E can be reasonably approximated by E_i, the incident x-ray beam energy. In the same way, in the energy range considered here, K-photoabsorption processes occur in Si and O atoms, giving rise to a total output electron energy which can also be assumed to be close to E_i. Then the application of the approximated law $D=K_0E_i^{\alpha}/\tau$ to each atomic species leads to a signal ratio defined in the following expression:

$$\frac{S_{AB}}{S_{SiO_2}}=\frac{(\mu/\tau)_A C'_A+(\mu/\tau)_B C'_B}{(\mu/\tau)_{SiO_2}}, \tag{5}$$

where C'_A is related to the weight percentage of the A component.

(ii) In another way, we can assume that the electronic current induced by escaping particles is essentially governed by the fastest primary electrons. For Fe, Ti, and Cu pre-edge, electron emissions are then clearly dominated by L photoelectrons (energy E_L), and the energy of LMM Auger electrons which complete the deexcitation step is about $E_L/10$. Thus, the output current can be written down as proportional to $[E_L^{3.2}\mu_L(E_i)]$. For Si and O atoms, there generally exists, within the energy range experimentally investigated here, a similar hierarchy between K photoelectrons (energy E_K) and KLL Auger electrons, except before the Ti K edge, where one must discuss further a possible noticeable contribution of KLL Auger electrons arising from Si atoms. Following these assumptions, the ratio expression becomes

$$\frac{S_{AB}}{S_{SiO_2}}=\frac{(\mu/\tau)_A C'_A(E_{AL}^{3.2})+(\mu/\tau)_B C'_B(E_{BL}^{3.2})}{(\mu/\tau)_{Si}C'_{Si}(E_{SiK}^{3.2})+(\mu/\tau)_O C'_O(E_{OK}^{3.2})}. \tag{6}$$

Using both formulas (5) and (6), numerical computations were performed and compared to experimental values. These results are quoted in Table III, as well as all parameters that have a direct connection with calculations. Absorption cross sections were collected in McMaster's table.[12]

Comparison between experimental and computed values clearly shows that assumption (i) is irrelevant to describe the behavior of the observed signal. On the other hand, assumption (ii) provides a very good fit with experimental data, especially for Fe- and Cu-based samples. However, we must introduce some additional corrections in order to describe accurately the Ti K pre-edge data; as mentioned above, Si atomic deexcitation yields KLL Auger electrons whose energy is about 1.6 keV. Compared to the K-photoelectron current, they theoretically yield a contribution which reaches the fraction of about $(1.6/3.1)^{3.2}$ (approximately 12%). This leads to a computed ratio decreasing from 1.83 to 1.71, a value which becomes more closely related to the experimental one. We may also recall that Ni-Ti alloys are amorphous, leading to a somewhat singular behavior of the conversion-electron EXAFS current, relative to those provided by crystals. This fact may preclude comparison between crystalline SiO_2 and amorphous Ti-Ni signals.

TABLE III. Experimental and computed pre-edge ratios S_{AB}/S_{SiO_2} and parameters required for analysis. C' is the weight concentration. 4.1(i): computation was performed by assuming that D must be explained in terms of the energy E_i exchanged during the photoabsorption event. 4.1(ii): computation was performed by assuming that D is essentially related to the fastest primary electrons. Comparison shows good agreement for the 4.1ii assumption: $D_p=KE_p^{2.2}$ must be defined for each primary electron kind.

	μ/τ	C'	E_i	E_L	(S_{AB}/S_{SiO_2})			E_i	Element	E_k	μ/τ
Sample	(cm^2/g)		(keV)	(keV)	4.1(i)	expt	4.1(ii)	(keV)		(keV)	(cm/g)
Fe_{60}	59	0.59	7.05	6.34	0.96	1.7	1.66	7.05	Si	5.2	95
Co_{40}	56	0.41		6.26					O	6.52	16.5
Ti_{50}	87	0.45	4.85	4.4	0.87	1.6	1.83	4.85	Si	3.1	263
Ni_{50}	188	0.55		4			(1.71)		O	4.4	49.4
Cu	38	1	8.95	8	1.55	2.10	2.10	8.95	Si	7.1	45
									O	8.5	6

B. Pre-edge slopes

As shown, for example on a Cu sample in Fig. 7, pre-edge data generally present a monotonically increasing variation versus x-ray energy, this behavior being far removed from the classical Victoreen law observed in transmission mode. Experimental slope values furnish a complementary test, allowing us to verify the validity of the empirical relations previously assumed. In accordance with Sec. IV A, one can disregard contributions of *LMM* Auger electrons so that for bulk samples (or very thick layers) Eq. (3) is reduced to

$$S=[kF(E_i)A(E_i)D(E_i)]/h_0 \ , \tag{7}$$

with $F(E_i)=E_p/E_i$, $E_p=E_i-E_L$, and $A(E)=\mu_{\text{sample}}(E_i)/\mu_{\text{Ne}}(E_i)$.

In order to perform unambiguous comparison between experimental and pre-edge slopes predicted here, one must also take into account external factors such as extra air beam absorption. Owing to the experimental setup configurations, a finite distance z_a crossed by the incoming x rays between the I_0 and I detections exists. This length was minimized to $z_a=6$ cm for EXAFS1 and EXAFS4 beam lines (Fe, Co, Ni, and Cu K edges) while $z_a=1$ cm for EXAFS3 beam line (Ti K edge). These path length values were used in the corrective terms introduced here. The proportional parameter k includes geometrical factors; in particular, it depends on the sample orientation with respect to the photon-beam direction, as well as the x-ray-irradiated surface. However, k is presumed x-ray-energy independent and one can eliminate it by analyzing the relative slope $S(E_i)/S(E_{i0})$, E_{i0} being chosen 0.2 keV below the K-edge jump.

Consequently, we are interested in the following derivative expression:

$$\frac{S'(E_{i0})}{S(E_{i0})}=\frac{F'(E_{i0})}{F(E_{i0})}+\frac{A'(E_{i0})}{A(E_{i0})}+\frac{\alpha}{E_{p0}}+z_\alpha\mu'_{\text{air}}(E_{i0}) \ . \tag{8}$$

The terms $(E_i-E_L)/E_i$ and $\mu_s(E_i)/\mu_{\text{Ne}}(E_i)$ present very smooth variations versus E_i and therefore they contribute slightly to the final relative slope. Yet, they have been estimated and resulting values are gathered in Table IV. Factors $A(E_i)$ and $\mu_{\text{air}}(E_i)$ were computed via the pre-edge data collected in McMaster's table and we fitted them by the usual Victoreen expression $(C/E^3+D/E^4)$; this yields the following D/C values: 0.04 (Ne), 0.32 (Ti), -0.7 (Fe), -1.22 (Ni), and -1.12 (Cu).

The examination of the two last columns in Table IV shows that the model correctly predicts the experimental slope behavior versus the nature of the atomic species that are probed. Moreover, theoretical slopes overestimate experimental ones because the conversion-electron detector generally provides a residual output current; its contribution to the measured signal decreases the relative slope and its correction leads to a better agreement with computation. For instance, accurate measurements performed at the Fe-K edge provide a dark-current contribution of about 10% of the total pre-edge signal; such an effect may become more important for light elements, because the pre-edge signal height becomes very weak.

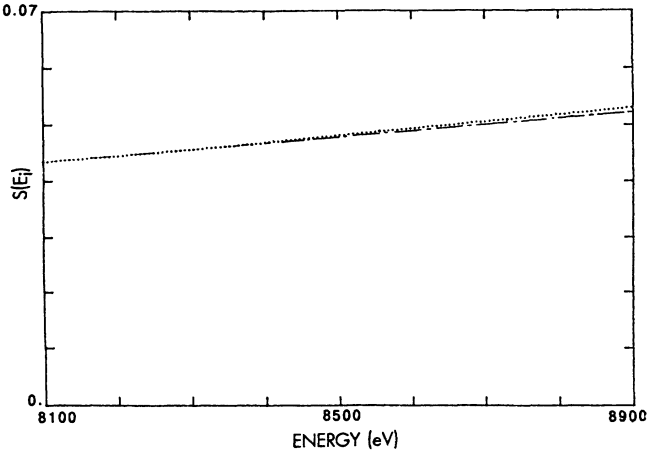

FIG. 7. Plot of pre-edge data (dot) vs photon energy below the Cu K edge for a 300-nm Cu-deposited thickness. Dashed line: linear fit.

V. CONCLUSION

The experimental results of the present paper agree with an exponential decay behavior of the conversion electron yield, as has been generally claimed in literature, when the initial absorption event occurred far from the free surface. This behavior is found to be a general feature within the 5–10-keV energy range examined here. Subsequently, it defines a sampling depth D which is atomic-species, composition, and structure dependent. Its magnitude relates directly to that of the electron scattering efficiency inside the probed materials. Extracted D values presented here cannot be directly compared with those obtained by other authors because their experimental setup was always different from the present one, measurements of electron yields being often performed in vacuum.[3,7] Moreover, some results[3] are related to experiments where one varies the thickness of an overlayer, the scattered electrons being then created inside a sublayer

TABLE IV. Comparison between calculated and experimental relative slopes S'/S (in keV^{-1} units) of pre-edge absorption signal vs the photon energy. Partial contributions of the different factors are also reported.

Element	E_{i0}(keV)	F'/F	A'/A	α/E_{p0}	$\mu'_{\text{air}}d$	S'/S_{cal}	S'/S_{expt}
Ti	4.8	0.01	0.01	0.49	0.02	0.54	0.49
Fe	7	0.01	0.015	0.34	0.02	0.39	0.35
Ni	8.2	0.01	0.02	0.29	0.01	0.33	0.31
Cu	8.8	0.01	0.02	0.27	0.01	0.31	0.27

constituted of a different atomic species. In the reverse case, as in our experiments, Martens and co-workers[7] probed samples at the absorption K edge of the overlayer itself by varying its thickness. Compared to the present curves, they obtained a singular behavior for thicknesses <25 nm. As discussed in Ref. 5, this phenomenon was attributed to secondary electrons induced by photoelectrons and *LMM* Auger electrons. This class of low-energy electrons must be taken into account if one uses a detector device working in vacuum, but for conversion-electron yield detectors working at atmospheric pressure, its weight is minimized compared to that related to *KLL* Auger electrons.

Indeed, several works[13] are related to fractional electron transmission for which authors have attempted to define a mass-thickness variable by using the relationship $\tau D = K_0 E_0^{\alpha}$, where E_0 is the incident electron energy. In the energy range quoted above, their fits yield an exponent coefficient α which varies from 1.2 to 1.7, depending on the definition used for τD. Following the definition of the Bethe range R_B,[14] a similar relation is obeyed, the index α being between 1.7 and 1.9. The discrepancy with the present value $\alpha = 2.2$ perhaps originates from experimental geometrical factors; in electron transmission experiments, incident electrons form a nearly parallel beam when they penetrate the matter while here, primary electrons are exited from excited centers, at random over 4π sr. Moreover, the present experiments measure a current corresponding to electrons scattered mainly in the forward direction. Transmission-thickness curves[13] become exponentially decreasing only for large thicknesses and present simultaneously a maximum and invariable most probable scattering angle; Bothe[15] presumed that this behavior corresponds to a random motion of individual electrons, a state which arises after a large number of scattering acts. Starting with a model in which electrons are incident from all directions, he derived an exponential transmission law with a thickness range proportional to E^2, an energy behavior which is close to the present experimental one.

Our results also confirm that scattering efficiency remains proportional to the matrix density, at least for cubic crystalline materials. Amorphous matter follows a singular behavior, but additional experiments are needed before considering it as a general feature.

Calculations performed in the previous section and discussion about relative current intensities and pre-edge slopes give some proof about the accuracy of the assumptions underlying the Eq. (1), in particular the E_p proportionality, which can be looked upon as a rather crude approximation. Therefore, because of effects seen in all the results, it becomes obvious that each primary electron is responsible for a specific contribution which is tightly related to its own energy. In most cases, the conversion-electron-yield signal can be reduced to the one induced by the most energetic primary electron, the other electrons produced during the absorption event generally providing a negligible current amount. To obtain more information about contributions of low-energetic electrons, in particular if the same expressions can still be applied with the coefficient $\alpha = 2.2$, experiments will be needed for very thin films of about 1 nm thickness.

[1]M. E. Kordesh and R. W. Hoffman, Phys. Rev. B **29**, 491 (1984).
[2]G. Tourillon, E. Dartyge, A. Fontaine, M. Lemonnier, and F. Bartol, Phys. Lett. A **121**, 251 (1987).
[3]W. T. Elam, J. P. Kirland, R. A. Neiser, and P. O. Wolf, Phys. Rev. B. **38**, 26 (1988).
[4]T. Guo and M. L. den Boer, Phys. Rev. B **31**, 6233 (1985).
[5]A. Erbill, G. S. Cargill III, R. Frahm, and R. F. Boehme, Phys. Rev. B **37**,2450 (1988).
[6]C. E. Bouldin, R. A. Forman, and M. I. Bell, Phys. Rev. B **35**, 1429 (1987).
[7]G. Martens, P. Rabe, G. Tolkiehn, and A. Werner, Phys. Status Solidi A **55**, 105 (1979).
[8]S. Michaux, M. Jaulin, G. Laplanche, and T. Delafond, Surf. Coat. Technol. **37**, 225 (1989).
[9]J. P. Riviere, Ph. Guesdon, J. Delafond, and M. F. Denanot, J. Less Common Met. **145**, 477 (1988).
[10]A. Naudon, J. Chihab, P. Goudeau, and J. Mimault, J. Appl. Crystallogr. **22**, 460 (1989).
[11]A. Naudon, T. Slimani, and Ph. Goudeau, J. Appl. Crystallogr. **24**, 501 (1991).
[12]W. H. McMaster, N. K. Del Grande, J. H. Mallet, and J. H. Hubell (unpublished).
[13]V. E. Coslett and R. N. Thomas, Br. J. Appl. Phys. **15**, 883 (1964); **15**, 1283 (1964).
[14]C. R. Worthington and S. G. Tomlin, Proc. Phys. Soc. London, **69**, 401 (1956).
[15]W. Bothe, Z. Phys. **54**, 161 (1929).